



Spectroscopic signature of spin triplet odd-valley superconductivity in two-dimensional materials

T. H. Kokkeler ^{1,2,*}, Chunli Huang ^{3,†}, F. S. Bergeret ^{4,1,‡} and I. V. Tokatly ^{5,1,6,§}

¹Donostia International Physics Center (DIPC), 20018 Donostia–San Sebastián, Spain

²Interfaces and Correlated Electron Systems, Faculty of Science and Technology, University of Twente, 7522 NB Enschede, The Netherlands

³Department of Physics and Astronomy, University of Kentucky, Lexington, Kentucky 40506-0055, USA

⁴Centro de Física de Materiales (CFM-MPC) Centro Mixto CSIC-UPV/EHU, E-20018 Donostia–San Sebastián, Spain

⁵IKERBASQUE, Basque Foundation for Science, 48009 Bilbao, Basque Country, Spain

⁶Nano-Bio Spectroscopy Group and European Theoretical Spectroscopy Facility (ETSF), Departamento de Polímeros y Materiales Avanzados: Física, Química y Tecnología, Universidad del País Vasco, 20018 Donostia–San Sebastián, Basque Country, Spain



(Received 25 May 2023; revised 1 August 2023; accepted 9 October 2023; published 8 November 2023)

Motivated by recent discoveries of superconductivity in lightly doped multilayer graphene systems, we present a low-energy model to study superconductivity in two-dimensional materials whose Fermi surface consists of two valleys at $\pm\mathbf{K}$ points. We assume a triplet odd-valley superconducting order with a pair potential that is isotropic in each valley but has a different sign in the two different valleys. Our theory predicts the emergence of an almost flat band of edge states centered at zero energy for certain edge orientations. As a result, a prominent experimental signature of this type of superconductivity is the presence of a large zero-energy peak in the local density of states near specific edges. The results of the effective low-energy theory are confirmed by numerically analyzing a specific microscopic tight-binding realization of odd-valley superconductivity: f -wave superconductivity on a honeycomb lattice in a ribbon geometry. Our work provides a test for odd-valley superconductivity through edge spectroscopy.

DOI: [10.1103/PhysRevB.108.L180504](https://doi.org/10.1103/PhysRevB.108.L180504)

Introduction. Superconductivity emerges in multilayer graphene stacks that are perturbed by a magic-angle twist potential [1–12] or by a strong electric displacement field [13–17]. These systems have received a lot of attention lately. However, it is still unclear if and how the superconducting order parameter Δ changes sign in its hexagonal Brillouin zones. The momentum dependence of the pair potential usually reflects the underlying pairing mechanism and thus can be used to constrain microscopic theories of superconductivity [18–26]. In this Letter, we identify a smoking-gun local tunneling spectroscopy signature to differentiate a spin-triplet odd-valley superconductor from a spin-singlet even-valley superconductor and illustrate it with a simple tight-binding model calculation.

The Fermi surface of lightly doped multilayer graphene systems is centered at the two valleys (K, K'), i.e., the two inequivalent corners of the hexagonal Brillouin zone. When Δ changes sign in a single valley and has nodal points on the Fermi surface, the density of states (DOS) decreases continuously to zero as the energy approaches the Fermi level. Such DOS profile can be probed by scanning-tunneling spectroscopy and leads to a V -shaped tunneling spectrum [27,28]. By contrast, if there are no nodes on the Fermi surface, it leads to the usual U -shaped local tunneling spectrum irrespective

of the relative sign of Δ in the two valleys because in either case the excitation energy of all Bogoliubov quasiparticles is gapped. However, as we demonstrate below, the superconducting gap of an odd-valley superconductor can close at the boundary of the two-dimensional materials, while the spectrum of an even-valley superconductor remains gapped. Moreover, the dispersion of the edge states in an odd-valley superconductor is anomalously flat, with $\omega \sim \Delta^2/\mu$, where μ is the chemical potential and these in-gap states lead to a large local DOS as shown in Fig. 1. On the contrary, for even-valley superconductors there are no edge states and a zero energy peak is absent; see Fig. 1. Since the LDOS can be probed using STM measurements, our calculations provide a tool for identifying odd-valley superconductivity.

In what follows, we calculate the edge state dispersion of a superconductor with spin-triplet odd-valley pairing, under the assumptions that $\Delta \ll \mu$ and that the Fermi surface consists of a single band. Using a universal property of Fermi liquids—the excitation energy is particle-hole symmetric at the Fermi surface—we demonstrate that the edge spectrum is macroscopically concentrated around zero energy. In the second part of the Letter, we use a tight-binding Hamiltonian to calculate the edge state dispersion and to confirm the results of our low-energy theory.

Low energy model. We start with a general 2D multiband superconductor described by the Hamiltonian

$$H = \sum_{\alpha} \begin{bmatrix} \xi_{\alpha,k} & \Delta_{\alpha,k} \\ \Delta_{\alpha,k} & -\xi_{\alpha,-k} \end{bmatrix} \otimes |u_{\alpha,k}\rangle \langle u_{\alpha,k}|. \quad (1)$$

*tim.kokkeler@dipc.org

†chunli.huang@uky.edu

‡fs.bergeret@csic.es

§ilya.tokatly@ehu.es

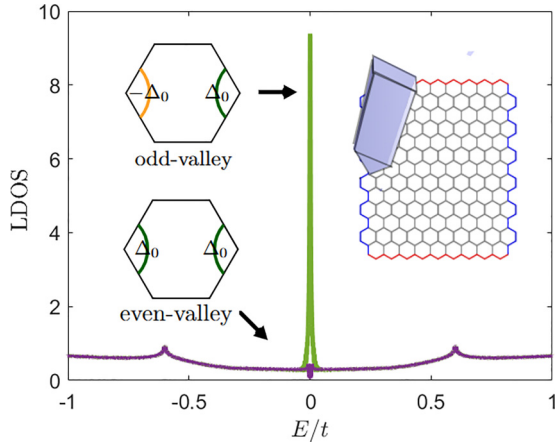


FIG. 1. Spin triplet odd-valley superconductivity in graphene leads to a large peak in the local density of states near armchair edges. The result is calculated using a tight-binding model presented later in the paper with superconducting-gap/Fermi energy $\Delta/\mu = 0.05$. Features at $\Delta/\mu \approx 0.6$ are not related to superconductivity but to the underlying band structure. The smearing parameter in the calculation of the density of states was set to $\delta/\Delta = 0.1$.

Here $\xi_{\alpha,k}$, $\Delta_{\alpha,k}$ are the quasiparticle energy and pair potential and α, \mathbf{k} are the band index and crystal momentum, respectively; $|u_{\alpha,k}\rangle\langle u_{\alpha,k}|$ is the band projector. The corresponding Green's function $G_{\mathbf{k}}(\omega) = (\omega - H)^{-1}$ in momentum space reads

$$G_{\mathbf{k}}(\omega) = \sum_{\alpha} \frac{(\omega \mathbf{1}_{\tau} - \xi_{\alpha,k} \tau_3 + \Delta_{\alpha,k} \tau_1)}{\omega^2 - \xi_{\alpha,k}^2 - \Delta_{\alpha,k}^2} \otimes |u_{\alpha,k}\rangle\langle u_{\alpha,k}|, \quad (2)$$

where τ_i ($i = 1, 2, 3$) and $\mathbf{1}_{\tau}$ are, respectively, the Pauli and the identity matrices spanning the Nambu space. We assume that the Fermi surface crosses only one of the bands and that the energy difference between bands is much larger than the pairing energy, such that interband correlations can be neglected.

We are interested in describing the bound states at the edge of an odd-valley superconductor, that is, a superconductor whose pair potential has a different sign in each valley. The sharp edge, located at the line $x = 0$, is modeled by adding to the periodic potential of the crystal a one-dimensional (1D) delta potential, $U(\mathbf{r}) = V\delta(x)\tau_3$, and taking the limit $V \rightarrow \infty$, which automatically imposes the wave functions to vanish at $x = 0$, effectively making it an edge.

Wave functions $|\psi(x)\rangle$ of the edge states are obtained using the Lippmann-Schwinger equation [29],

$$|\psi(x)\rangle = V\tau_3 G_{x,k_y}(\omega) |\psi(x=0)\rangle. \quad (3)$$

Here G_{x,k_y} is the Fourier transform, with respect to $k_x \rightarrow x$, of the Green's function in Eq. (2):

$$G_{x,k_y}(\omega) = \int_{\text{BZ}} e^{ik_x x} G_{k_x, k_y}(\omega) \frac{dk_x}{2\pi}. \quad (4)$$

From Eq. (3), the energy of the bound states is determined by the equation

$$\det[V^{-1} - \tau_3 G_{x=0, k_y}(\omega)] = 0. \quad (5)$$

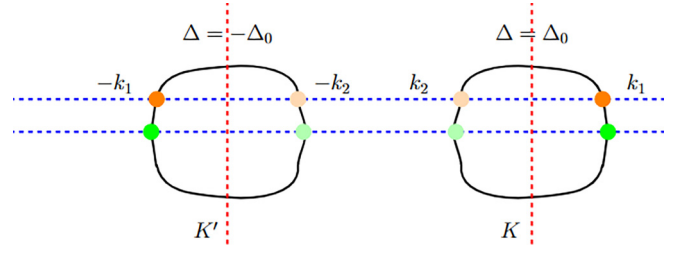


FIG. 2. Schematic of a Fermi surface with two disconnected components and an odd-valley pair potential. The dashed lines correspond to integration lines for the Fourier transforms. The orientation of the edge determines which integration line should be taken. The blue lines cross both valleys and thus edges with this orientation will have edge states. The red lines cross only one valley and therefore edges with this orientation do not exhibit edge states.

Equations (3) and (5) depend parametrically on k_y . This dependence determines the dispersion of the edge states. In order to solve this equation and then construct the wave function of the edge states, one needs to evaluate the integral in Eq. (4). The integration runs over k_x at fixed k_y , i.e., over straight lines in k space. By assumption, the Fermi surface consists of two disconnected pockets (valleys) surrounding two distinct points in the Brillouin zone \mathbf{K} and $-\mathbf{K}$, related by the inversion operation, as typically occurs in graphene-related materials; see Fig. 2. The shape of the Fermi surfaces around these two points is arbitrary. We assume that the pair potential is constant within a single valley, but changes sign between the valleys. As mentioned above, due to the Pauli exclusion principle, this odd-valley superconductivity corresponds to a triplet state [30].

When the pair potential is much smaller than both the Fermi energy, $\Delta \ll \mu$ [13,14], and the energy separation from other bands, the integral in Eq. (4) is dominated by the band crossing the Fermi level and all remote bands may be ignored. We therefore leave only this relevant band in the Green's function of Eq. (2) and everywhere below drop the band index by writing $|u_{\mathbf{k}}\rangle$, $\xi_{\mathbf{k}}$, and $\Delta_{\mathbf{k}}$.

The result of the integration depends on the orientation of the integration lines in k space, which, in turn, are determined by the normal to the edge as by construction they are orthogonal to the x axis. We focus here on two edge orientations, indicated by the red and blue lines in Fig. 2. In the case of graphene they correspond to zigzag and armchair edges, respectively; see Fig. 1. In the red case, the integration lines may cross the Fermi contour only in a single valley. Because the pair potential is assumed to be isotropic across the valley, this situation is equivalent to the edge of a conventional s -wave superconductor and therefore the system does not exhibit edge states at such edges.

More interesting is the orientation of the edge corresponding to the blue lines in Fig. 2. In this case, the integration line may cross neither or both valleys. In the former case, one can verify from the Lippmann-Schwinger equation that no edge states appear. Therefore, we focus on values of k_y for which the integration line crosses both valleys.

To compute the integral over k_x we notice that in the case $\Delta \ll \mu$ the main contribution is from momenta close to the Fermi momentum. Therefore, under the standard assumptions

of Fermi liquid theory, we linearize the spectrum around the points \mathbf{k}_n , where the integration line crosses the Fermi contour. As a result, the integral in Eq. (4) is transformed to the sum of the integrals over ξ_{k_n} at each crossing point. Specifically, $G_{x=0,k_y}(\omega)$ is given by

$$G_{x=0,k_y} \approx - \sum_{n=1,2} \frac{1}{2v_n} \frac{\omega}{\sqrt{\Delta^2 - \omega^2}} \mathbf{1}_\tau \otimes |u_{k_n}\rangle\langle u_{k_n}|, \quad (6)$$

where $v_{1,2} = |\partial\xi_k/\partial k_x|_{k_{1,2}}$ are x components of the Fermi velocities at the points $\mathbf{k}_{1,2}$ at which the integration line crosses the Fermi contour in the K valley; see Fig. 2. Thus, at $x = 0$, the Green's function is proportional to the unit matrix in Nambu space and comes from the term $\sim \omega \mathbf{1}_\tau$ in Eq. (2). The term $\sim \xi_k \tau_3$ vanishes upon ξ integration due to the particle-hole symmetry inherent to the linearized spectrum. Finally, the $\Delta_k \tau_1$ contribution vanishes after summation over the valleys due to the valley antisymmetry of the pairing potential.

By substituting Eq. (6) into Eq. (3) at $x = 0$ and projecting it onto the Bloch states $|u_{k_1}\rangle$ and $|u_{k_2}\rangle$, we get a 4×4 problem for two Nambu spinors $\langle u_{k_{1,2}} | \psi(0) \rangle$. By evaluating the determinant of the corresponding 4×4 matrix in Eq. (5) and taking the limit $V \rightarrow \infty$, it follows that there exist four edge states with $\omega(k_y) = 0$, for all k_y . Importantly, the zero energy of the edge states and the absence of dispersion, while true with very high accuracy, is nonetheless an approximate property. It is a consequence of the approximate electron-hole symmetry that is controlled by the parameter $\frac{\Delta}{\mu} \ll 1$.

To find the wave functions of the edge states we compute $G_{x,k_y}(\omega)$ using the same approximations and insert the result into Eq. (3). This yields four states which in the limit $V \rightarrow \infty$ naturally split into two pairs of states localized on the opposite sides of the barrier. The wave functions of these four edge states with energies $\omega(k_y) = 0 + O(\Delta^2/\mu)$ read

$$\begin{aligned} \Psi_{L1,2} = & \left(\sin k_{1,2} x \begin{bmatrix} 1 \\ \pm i \end{bmatrix} \otimes |u_{k_{1,2}}\rangle e^{\kappa_{1,2} x} \right. \\ & \left. + \sin k_{2,1} x \langle u_{k_{2,1}} | u_{k_{1,2}} \rangle \begin{bmatrix} 1 \\ \mp i \end{bmatrix} \otimes |u_{k_{2,1}}\rangle e^{\kappa_{2,1} x} \right) \Theta(-x), \end{aligned} \quad (7)$$

$$\begin{aligned} \Psi_{R1,2} = & \left(\sin k_{1,2} x \begin{bmatrix} 1 \\ \mp i \end{bmatrix} \otimes |u_{k_{1,2}}\rangle e^{-\kappa_{1,2} x} \right. \\ & \left. + \sin k_{2,1} x \langle u_{k_{2,1}} | u_{k_{1,2}} \rangle \begin{bmatrix} 1 \\ \pm i \end{bmatrix} \otimes |u_{k_{2,1}}\rangle e^{-\kappa_{2,1} x} \right) \Theta(x), \end{aligned} \quad (8)$$

where the upper sign in \pm, \mp corresponds to $\Psi_{L,R1}$ and the lower sign to $\Psi_{L,R2}$ and where $\kappa_n = \sqrt{\Delta^2 - \omega^2}/v_n$. The states $\Psi_{L1,2}$ and $\Psi_{R1,2}$ are localized on the left and right side of the potential wall, respectively, as indicated by the Heaviside functions $\Theta(\mp x)$. Therefore, to the leading order in $\Delta/\mu \ll 1$, each physical edge supports two degenerate zero energy edge states for each k_y . Lifting the degeneracy and the appearance of a weak dispersion as a higher order effect in Δ/μ is analyzed in detail in the Supplemental Material [31] and also discussed below for a specific lattice model of an odd-valley superconductor.

The above results can be directly applied to graphene or other materials with hexagonal lattices. Armchair edges with $\Delta\mathbf{K} = 2K_x \hat{x}$ correspond to the blue integration lines in Fig. 2. In this case, our theory predicts the existence of a flat band of zero-energy edge states. This will manifest as a large peak in the density of states, localized at the edge over a coherence length. On the other hand, zigzag edges with $\Delta\mathbf{K} = 2K_y \hat{y}$ correspond to the red integration lines in Fig. 2. In this case, no edge states are expected. We emphasize that this difference between armchair and zigzag edges is due to the normal of the surface being parallel or perpendicular to the $K - K'$ line, not to the exact shape of the edges. These two features can be used to unequivocally characterize the odd-valley superconductivity in graphenelike materials. The superconductors described by our low-energy model are topologically trivial, since though they are odd parity, the Fermi surface does not enclose time-reversal invariant momenta [32]. If additionally mirror symmetry is present, the superconductors may have a mirror topology, such as in odd-layer graphene stacks [33].

Lattice model. As a microscopic illustration of the above low-energy theory, we use a specific lattice realization of an odd-valley superconductor to demonstrate the appearance of the massively degenerate edge states. We focus on a honeycomb tight-binding lattice and consider a ribbon with infinite extension in the y direction and restricted by two armchair edges in the x direction. In order to generate an effective odd-valley superconducting order parameter, we consider pairing only in the next-nearest (AA) sublattice. This type of intrasublattice pairing potential has been microscopically studied in Refs. [19,34].

We consider spinless electrons. The Hamiltonian for a given Bloch momentum k_y reads

$$\begin{aligned} H(k_y) = & \sum_i -\mu (a_{i,k_y}^\dagger a_{i,k_y} + b_{i,k_y}^\dagger b_{i,k_y}) \\ & + t (e^{-ik_y} a_{i,k_y}^\dagger b_{i,k_y} + e^{i\frac{1}{2}k_y} a_{i,k_y}^\dagger b_{i+1,k_y} + e^{i\frac{1}{2}k_y} a_{i,k_y}^\dagger b_{i-1,k_y}) \\ & + \Delta \left[(a_{i-2,k_y}^\dagger a_{i,k_y}^\dagger - a_{i+2,k_y}^\dagger a_{i,k_y}^\dagger) \right. \\ & + \left(-2 \cos \frac{3}{2} k_y \right) (a_{i-1,k_y}^\dagger a_{i,k_y}^\dagger - a_{i+1,k_y}^\dagger a_{i,k_y}^\dagger) \\ & + (b_{i-2,k_y}^\dagger b_{i,k_y}^\dagger - b_{i+2,k_y}^\dagger b_{i,k_y}^\dagger) \\ & \left. + \left(-2 \cos \frac{3}{2} k_y \right) (b_{i-1,k_y}^\dagger b_{i,k_y}^\dagger - b_{i+1,k_y}^\dagger b_{i,k_y}^\dagger) \right] \\ & + \text{H.c.}, \end{aligned} \quad (9)$$

where the summation index i runs over all unit cells from $i = 1$ to $i = 1024$, a_i and b_i are annihilation operators in unit cell i on sublattices A and B , respectively, μ is the chemical potential, Δ_0 is the pair potential, and $\delta_1 = a(0, -1)$, $\delta_2 = \frac{a}{2}(\sqrt{3}, 1)$, $\delta_3 = \frac{a}{2}(-\sqrt{3}, 1)$ are vectors between nearest neighbors, while $\chi_1 = \delta_3 - \delta_2$, $\chi_2 = \delta_1 - \delta_3$, $\chi_3 = \delta_2 - \delta_1$ are vectors between next-nearest neighbors. This model leads to f -wave superconductivity, studied in Refs. [35–40]. As shown in the Supplemental Material [31], the tight-binding Hamiltonian, Eq. (9), reduces to the low-energy model in Eq. (1) in the

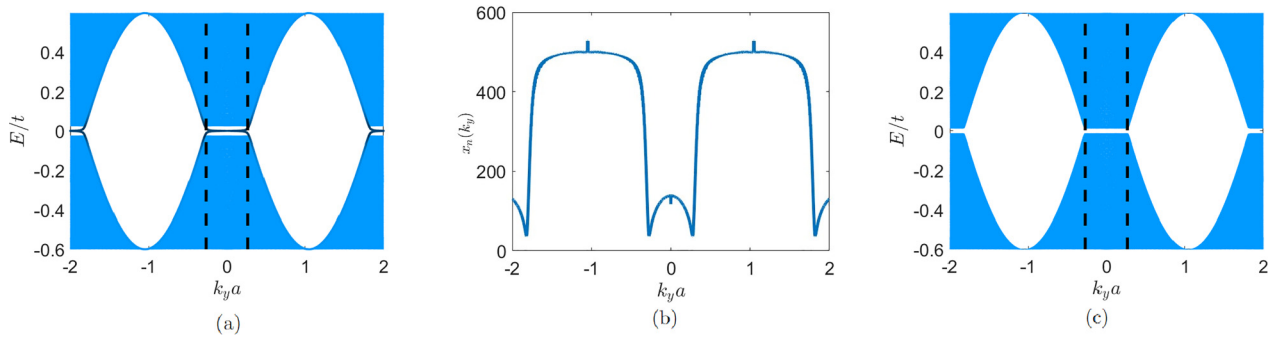


FIG. 3. (a) Dispersion for odd-valley superconductivity calculated using the tight-binding model for $\Delta/\mu = 0.05$ and $\mu/t = 0.4$, plotted over one full Brillouin zone. The edge states are clearly separated in energy from the other states. They are flat near $k_y = 0$ and merge with the band near $k_y = k_F$, indicated by the dashed lines. (b) The average value of the position operator for the edge states as a function of k_y . The states are well localized for $k_y \ll k_F$, indicated by the dashed lines in panel (a). The localization length is smallest near the Fermi surface $k_y = k_F$ and the states become delocalized as their energy approaches the bulk gap for $k_y > k_F$. Here a is the carbon-carbon distance. (c) Dispersion for even-valley superconductivity calculated using the tight-binding model for $\Delta/\mu = 0.05$ and $\mu/t = 0.4$. The bulk dispersion is similar to odd-valley superconductivity, but edge states are absent.

limit $t \gg \mu \gg \Delta$. For this model the band projectors $|u_k\rangle\langle u_k|$ are given by $\frac{1}{2}(\mathbf{1} + \frac{k_x}{\sqrt{k_x^2 + k_y^2}}\rho_x + \frac{k_y}{\sqrt{k_x^2 + k_y^2}}\rho_y)$, where $\rho_{x,y}$ are the first and second Pauli matrix in sublattice space.

Figure 3(a) shows the energy dispersion $E_n(k_y)$ vs k_y of our Hamiltonian, Eq. (9). The bulk spectrum (blue region) is gapped, with a gap of the order of Δ , and the edge states form an almost flat band around zero energy in the gap. As indicated using the dashed lines in 3(a), the flat band is well separated from the bulk for $k_y < k_F$ and merges with the bulk bands for $k_y \gg k_F$. The small dispersion of the edge states for $k_y \ll k_F$ in Fig. 3(a) arises from particle-hole asymmetry which is controlled by the small parameter $\frac{\Delta}{\mu}$. This parameter is truly small for superconductors observed reported for Bernal bilayer graphene and rhombohedral trilayer graphene in Refs. [13,14], where $T_c/T_F \sim 10^{-3}$. We set $\frac{\Delta}{\mu} = 0.05$ and $\frac{\mu}{t} = 0.4$ in our numerical calculations. The result of this almost flat band is a strongly enhanced local density of states close to zero energy, as shown in Fig. 1.

Next, we compute the expectation value of the position operator for the eigenstate $\psi_{k_y,n}$:

$$x_n(k_y) = \frac{\int x |\psi_{k_y,n}|^2 dx}{a \int |\psi_{k_y,n}|^2 dx}, \quad (10)$$

where a is the carbon-carbon distance in our honeycomb lattice. Figure 3(b) shows $x_0(k_y)$ vs k_y , where $n = 0$ labels the positive energy states inside the superconducting gap. $x_0(k_y)$ is inversely correlated to the energy difference between the edge states and the bulk-state continuum. For $k_y \ll k_F$, $x_0(k_y)$ is very small compared to the width of the ribbon. In fact, $x_0(k_y = 0) \sim t/\Delta$ and $x_0(k_y = k_F) \sim t(\Delta\mu)^{-1/2}$; see the Supplemental Material [31]. In Fig. 3(c) we show that in-gap states are absent in the case of even-valley superconductivity, while the bulk spectrum is similar. This leads to the absence of a zero energy peak in the density of states as shown in Fig. 1, confirming that the presence of a zero-energy peak signals unconventional superconductivity.

Since the ribbon Hamiltonian we consider is invariant under the mirror plane $H(k_y) = H(-k_y)$, the counterpropa-

gating edge states are located on the same position: $x_0(k_y) = x_0(-k_y)$. We found generic disorder-induced transition matrix elements between them are finite $\langle \psi_{0,k_y} | \tau_3 V | \psi_{0,-k_y} \rangle \neq 0$, so the counterpropagating edge states will in fact be affected by edge imperfections. We may distinguish between smooth and sharp disorder. The states are robust against smooth disorder, since this does not mix the opposite valleys and thus leaves our conclusions unaltered. Sharp disorder such as vacancies on the other hand have zero-energy states themselves following a mechanism very similar to edges. Therefore, as long as their density is not too high, the zero energy peak in the density of states remains. We also verified numerically using our tight-binding model that the resulting energy shift of the bound states is small as long as the density of edge vacancies is not too large. Thus the large zero energy peak is robust against edge impurities.

Conclusions. We have presented an effective low-energy theory to analyze odd-valley superconductivity in 2D materials that have a Fermi surface split into two valleys. This type of unconventional pairing is allowed by symmetry and involves an odd-parity pair potential that has an opposite sign in different valleys but remains isotropic within each valley. Our model predicts the existence of an almost flat band of edge states if the normal to the edge is such that the integration line in k space passes through both valleys. To confirm this prediction, we have also studied a tight-binding Hamiltonian for f -wave superconductivity in honeycomb lattices. Our findings showed massively degenerate edge states that appear as a pronounced zero energy peak in the density of states accessible through local spectroscopic techniques.

Our study has broad applicability to materials with hexagonal or triangular lattices, including graphene, NbSe, MoS₂ [41], nitrides [42,43], germanene [44], and silicene [45].

Acknowledgments. We would like to thank S. Nadj-Perge, F. Guinea, M. A. Cazalilla, A. A. Golubov, A. H. MacDonald, A. Vishwanath, and S. Suzuki for useful discussions. T.K. and S.B. acknowledge financial support from Spanish MCIN/AEI/10.13039/501100011033 through

Projects No. PID2020-114252GB-I00 (SPIRIT) and No. TED2021-130292B-C42, the Basque Government through Grant No. IT-1591-22, and European Union's Horizon 2020 Research and Innovation Framework Programme under Grant

No. 800923 (SUPERTED). I.V.T. acknowledges support by Grupos Consolidados UPV/EHU del Gobierno Vasco (Grant No. IT1453-22) and by Grant No. PID2020-112811GB-I00 funded by MCIN/AEI/10.13039/501100011033.

- [1] Y. Cao, V. Fatemi, S. Fang, K. Watanabe, T. Taniguchi, E. Kaxiras, and P. Jarillo-Herrero, *Nature (London)* **556**, 43 (2018).
- [2] X. Lu, P. Stepanov, W. Yang, M. Xie, M. A. Aamir, I. Das, C. Urgell, K. Watanabe, T. Taniguchi, G. Zhang *et al.*, *Nature (London)* **574**, 653 (2019).
- [3] P. Stepanov, I. Das, X. Lu, A. Fahimniya, K. Watanabe, T. Taniguchi, F. H. Koppens, J. Lischner, L. Levitov, and D. K. Efetov, *Nature (London)* **583**, 375 (2020).
- [4] A. L. Szabó and B. Roy, *Phys. Rev. B* **105**, L081407 (2022).
- [5] M. Yankowitz, S. Chen, H. Polshyn, Y. Zhang, K. Watanabe, T. Taniguchi, D. Graf, A. F. Young, and C. R. Dean, *Science* **363**, 1059 (2019).
- [6] B. Lian, Z. Wang, and B. A. Bernevig, *Phys. Rev. Lett.* **122**, 257002 (2019).
- [7] J. M. Park, Y. Cao, L.-Q. Xia, S. Sun, K. Watanabe, T. Taniguchi, and P. Jarillo-Herrero, *Nat. Mater.* **21**, 877 (2022).
- [8] Z. Hao, A. Zimmerman, P. Ledwith, E. Khalaf, D. H. Najafabadi, K. Watanabe, T. Taniguchi, A. Vishwanath, and P. Kim, *Science* **371**, 1133 (2021).
- [9] Y. Zhang, R. Polski, C. Lewandowski, A. Thomson, Y. Peng, Y. Choi, H. Kim, K. Watanabe, T. Taniguchi, J. Alicea *et al.*, *Science* **377**, 1538 (2022).
- [10] G. Chen, A. L. Sharpe, P. Gallagher, I. T. Rosen, E. J. Fox, L. Jiang, B. Lyu, H. Li, K. Watanabe, T. Taniguchi *et al.*, *Nature (London)* **572**, 215 (2019).
- [11] J. M. Park, Y. Cao, K. Watanabe, T. Taniguchi, and P. Jarillo-Herrero, *Nature (London)* **590**, 249 (2021).
- [12] J. M. Park, Y. Cao, L. Xia, S. Sun, K. Watanabe, T. Taniguchi, and P. Jarillo-Herrero, [arXiv:2112.10760](https://arxiv.org/abs/2112.10760).
- [13] H. Zhou, T. Xie, T. Taniguchi, K. Watanabe, and A. F. Young, *Nature (London)* **598**, 434 (2021).
- [14] H. Zhou, L. Holleis, Y. Saito, L. Cohen, W. Huynh, C. L. Patterson, F. Yang, T. Taniguchi, K. Watanabe, and A. F. Young, *Science* **375**, 774 (2022).
- [15] L. Holleis, C. L. Patterson, Y. Zhang, H. M. Yoo, H. Zhou, T. Taniguchi, K. Watanabe, S. Nadj-Perge, and A. F. Young, [arXiv:2303.00742](https://arxiv.org/abs/2303.00742).
- [16] Y. Zhang, R. Polski, A. Thomson, É. Lantagne-Hurtubise, C. Lewandowski, H. Zhou, K. Watanabe, T. Taniguchi, J. Alicea, and S. Nadj-Perge, *Nature (London)* **613**, 268 (2023).
- [17] T. T. Heikkilä, *Science* **375**, 719 (2022).
- [18] D. J. Scalapino, *Rev. Mod. Phys.* **84**, 1383 (2012).
- [19] V. Crépel, T. Cea, L. Fu, and F. Guinea, *Phys. Rev. B* **105**, 094506 (2022).
- [20] T. Cea, P. A. Pantaleón, V. T. Phong, and F. Guinea, *Phys. Rev. B* **105**, 075432 (2022).
- [21] T. Cea, *Phys. Rev. B* **107**, L041111 (2023).
- [22] P. A. Pantaleon, A. Jimeno-Pozo, H. Sainz-Cruz, T. Cea, V. T. Phong, and F. Guinea, *Nat. Rev. Phys.* **5**, 304 (2023).
- [23] A. Ghazaryan, T. Holder, M. Serbyn, and E. Berg, *Phys. Rev. Lett.* **127**, 247001 (2021).
- [24] A. Jimeno-Pozo, H. Sainz-Cruz, T. Cea, P. A. Pantaleón, and F. Guinea, *Phys. Rev. B* **107**, L161106 (2023).
- [25] H. Sainz-Cruz, P. A. Pantaleón, V. T. Phong, A. Jimeno-Pozo, and F. Guinea, *Phys. Rev. Lett.* **131**, 016003 (2023).
- [26] F. Guinea and B. Uchoa, *Phys. Rev. B* **86**, 134521 (2012).
- [27] S. Kashiwaya and Y. Tanaka, *Rep. Prog. Phys.* **63**, 1641 (2000).
- [28] H. Kim, Y. Choi, C. Lewandowski, A. Thomson, Y. Zhang, R. Polski, K. Watanabe, T. Taniguchi, J. Alicea, and S. Nadj-Perge, *Nature (London)* **606**, 494 (2022).
- [29] B. A. Lippmann and J. Schwinger, *Phys. Rev.* **79**, 469 (1950).
- [30] The two valleys are centered at $\pm K$ points in the Brillouin zone so that the triplet odd-valley pair potential is odd parity, that is, $\Delta[-(\mathbf{K} + \delta\mathbf{k})] = -\Delta(\mathbf{K} + \delta\mathbf{k})$. This distinguishes this type of superconductivity from multiorbital superconductivity with s_{\pm} pairing [32,46,49–51], which is predicted to exist in pnictides [47,48].
- [31] See Supplemental Material at <http://link.aps.org/supplemental/10.1103/PhysRevB.108.L180504> for a detailed description of the tight-binding model, a proof that the low-energy model discussed in this paper is the correct low-energy approximation of this tight-binding model, and for analytical solutions in certain limiting cases.
- [32] M. Sato, Y. Tanaka, K. Yada, and T. Yokoyama, *Phys. Rev. B* **83**, 224511 (2011).
- [33] V. T. Phong, H. Sainz-Cruz, E. J. Mele, and F. Guinea, [arXiv:2307.03031](https://arxiv.org/abs/2307.03031).
- [34] C. Huang, N. Wei, W. Qin, and A. H. MacDonald, *Phys. Rev. Lett.* **129**, 187001 (2022).
- [35] H. Goudarzi and M. Khezerlou, *Physica E* **44**, 2082 (2012).
- [36] Y.-Z. Chou, F. Wu, J. D. Sau, and S. Das Sarma, *Phys. Rev. Lett.* **127**, 187001 (2021).
- [37] Y.-Z. Chou, F. Wu, J. D. Sau, and S. Das Sarma, *Phys. Rev. B* **105**, L100503 (2022).
- [38] Y.-Z. Chou, F. Wu, J. D. Sau, and S. Das Sarma, *Phys. Rev. Lett.* **127**, 217001 (2021).
- [39] E. Pangburn, L. Haurie, A. Crépieux, O. A. Awoga, A. M. Black-Schaffer, C. Pépin, and C. Bena, [arXiv:2211.05146](https://arxiv.org/abs/2211.05146).
- [40] E. Pangburn, L. Haurie, A. Crépieux, O. A. Awoga, N. Sedlmayr, A. M. Black-Schaffer, C. Pépin, and C. Bena, [arXiv:2212.07445](https://arxiv.org/abs/2212.07445).
- [41] J. Lu, O. Zheliuk, I. Leermakers, N. F. Yuan, U. Zeitler, K. T. Law, and J. Ye, *Science* **350**, 1353 (2015).
- [42] S. Yamanaka, H. Kawaji, K.-i. Hotehama, and M. Ohashi, *Adv. Mater.* **8**, 771 (1996).
- [43] S. Yamanaka, K.-i. Hotehama, and H. Kawaji, *Nature (London)* **392**, 580 (1998).
- [44] Y. Xi, X. Jing, Z. Xu, N. Liu, Y. Liu, M.-L. Lin, M. Yang, Y. Sun, J. Zhuang, X. Xu *et al.*, *J. Am. Chem. Soc.* **144**, 18887 (2022).
- [45] J. Zhao, H. Liu, Z. Yu, R. Quhe, S. Zhou, Y. Wang, C. C. Liu, H. Zhong, N. Han, J. Lu *et al.*, *Prog. Mater. Sci.* **83**, 24 (2016).

- [46] Y. Fukaya, S. Tamura, K. Yada, Y. Tanaka, P. Gentile, and M. Cuoco, *Phys. Rev. B* **97**, 174522 (2018).
- [47] A. A. Golubov, A. Brinkman, Y. Tanaka, I. I. Mazin, and O. V. Dolgov, *Phys. Rev. Lett.* **103**, 077003 (2009).
- [48] M. Mashkooi, A. G. Moghaddam, M. H. Hajibabae, A. M. Black-Schaffer, and F. Parhizgar, *Phys. Rev. B* **99**, 014508 (2019).
- [49] A. V. Burmistrova, I. A. Devyatov, A. A. Golubov, K. Yada, Y. Tanaka, M. Tortello, R. S. Gonnelli, V. A. Stepanov, X. Ding, H.-H. Wen, and L. H. Greene, *Phys. Rev. B* **91**, 214501 (2015).
- [50] S. Onari and Y. Tanaka, *Phys. Rev. B* **79**, 174526 (2009).
- [51] A. V. Burmistrova, I. A. Devyatov, A. A. Golubov, K. Yada, and Y. Tanaka, *J. Phys. Soc. Jpn.* **82**, 034716 (2013).